Science Advances

AAAS

advances.sciencemag.org/cgi/content/full/1/9/e1500640/DC1

Supplementary Materials for

Persistent optical gating of a topological insulator

Andrew L. Yeats, Yu Pan, Anthony Richardella, Peter J. Mintun, Nitin Samarth, David D. Awschalom

Published 9 October 2015, *Sci. Adv.* **1**, e1500640 (2015)
DOI: 10.1126/sciadv.1500640

The PDF file includes:

Supplementary Materials

§ S1. Persistence of the Optical Gating Effect for 16 Hours

The persistence of the optical gating effect is characterized in Figure S1. The longitudinal resistance of a Hall bar geometry sample is monitored at 3 K under illumination by UV or red light. Before measurement, the sample was exposed to red light to initialize it into the *p*-type state. At $t = 0$ hours the sample was exposed to UV light ($\lambda = 375$ nm, $I = 1$ mW/m^2, $t = 100$ s) in order to gate the film to a chemical potential near the charge neutrality point. This causes the resistance to increase from 6.7 to 16 kΩ. After initial transients, the resistance remains at its new value for 16 hours with little sign of relaxation. At $t =$ 16 hours, red light ($\lambda = 635$ nm, $I = 45$ W/m^2, $t = 550$ s) was used to return the sample to its initial state.

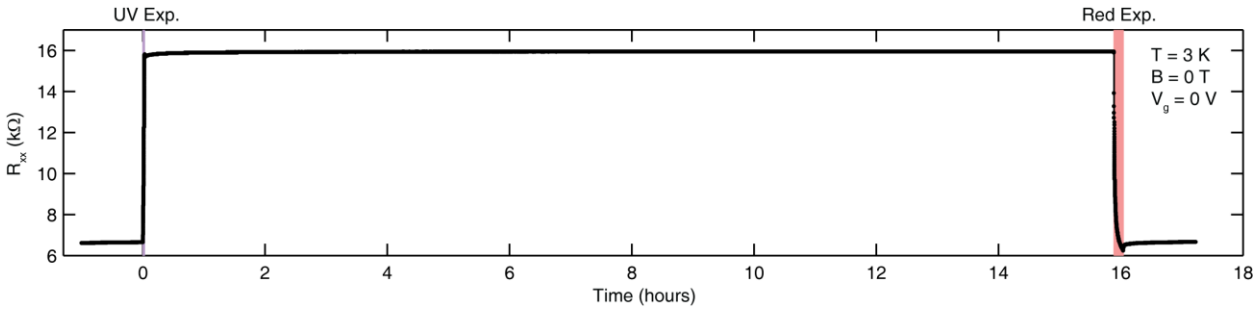

Figure S1. Persistence of the optical gating effect for 16 hours. Longitudinal resistance R_{xx} is plotted as a function of time during illumination by UV (purple highlighting) or red (pink highlighting) light, showing the persistence of the optical gating effect for 16 hours.

§ S2. Superposition of Electrostatic and Optical Gating

Giant increases in dielectric constant have been reported in $SrTiO_3$ at low temperature under illumination by UV light and are sometimes associated with ferroelectric-like phenomena(*42-44*). Changes in dielectric constant of the substrate material would affect the efficiency of the electrostatic back-gating response of our samples. We have not observed large changes in electrostatic gating strength after UV illumination at low temperature. This suggests the optical gating effect we observe primarily superposes with, rather than modifies, electrostatic gating. This is consistent with a defect-mediated optical gating mechanism. Figure S2A shows the longitudinal resistance of a $(Bi,Sb)_2Te_3/SrTiO_3$ heterostructure measured in the Van der Pauw geometry as a function of electrostatic back-gate voltage. The numerical derivative of this curve (Figure S2C) characterizes the strength of the electrostatic gating effect. Figure S2B shows the evolution of longitudinal resistance after consecutive exposures to UV light. Between each exposure, the back gate voltage was ramped between ±1 V and the slope measured to characterize how the strength of the electrostatic gating effect may change after UV exposure. These slope values are plotted in Figure S2D, and show reasonable agreement with the all-electrostatic data in Figure S2C.

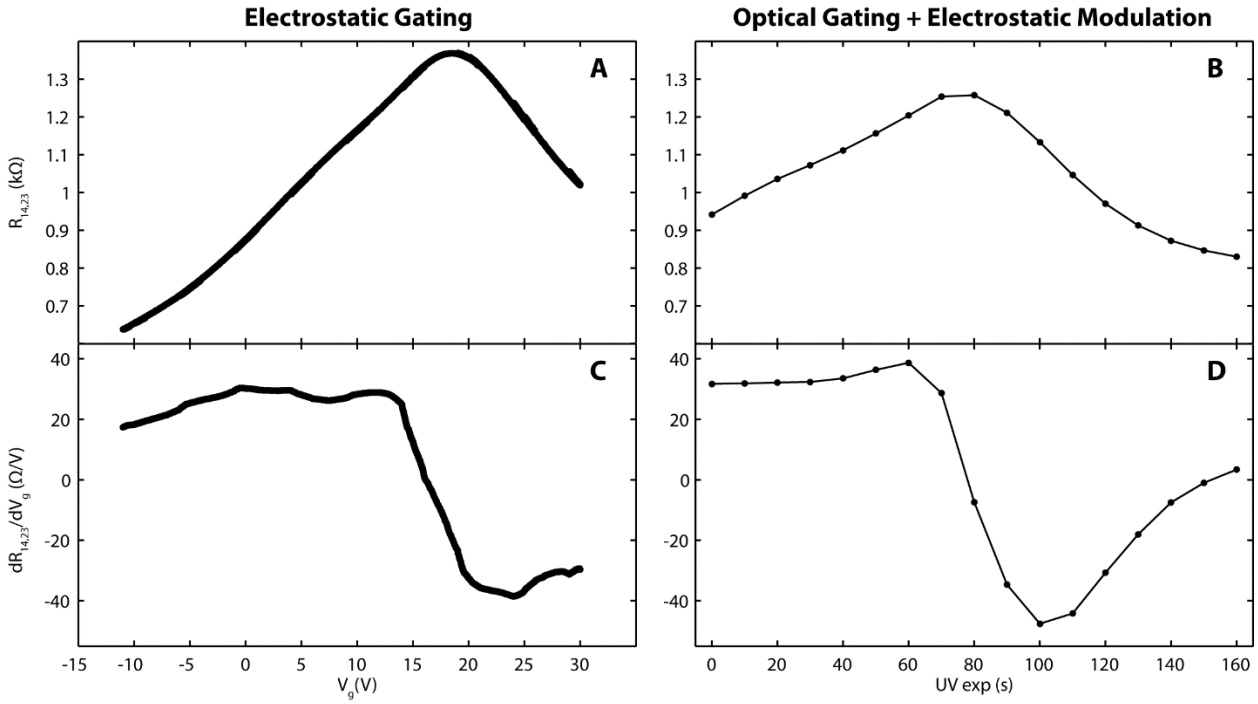

Figure S2. Superposition of electrostatic and optical gating. (A) Longitudinal resistance of a Van der Pauw geometry sample $R_{14,23}$ as a function of back-gate voltage V_g without illumination. **(B)** Longitudinal resistance of the same sample measured at V_g = 0 V after consecutive exposures to UV light. **(C)** Numerical derivative of (A), $dR_{14,23}/dV_g$, characterizing the strength of the electrostatic gating effect. **(D)** Electrostatic gating strength measured after successive UV exposure by ramping between V_g = ±1 V and recording the resulting slope $dR_{14,23}/dV_g$.

§ S3. Optical Gating of ≈ 50-nm Sputtered ZnO Film on $SrTiO_3$

To demonstrate the generalizability of the optical gating effect to other materials systems, a 50 nm layer of ZnO was deposited onto a (111) $SrTiO_3$ substrate by RF sputtering. The deposition was performed at 100 W with an Ar pressure of 3 mTorr. Figure S3 shows the longitudinal resistance of this film after exposure to UV or red light, showing a persistent bidirectional response analogous to the optical gating effect seen in $(Bi,Sb)_2Te_3/SrTiO_3$ heterostructures. The sign of the response is consistent with an *n*-type film. This suggests that the optical gating effect may be applicable to a wide variety of electronic materials grown or deposited on $SrTiO_3$.

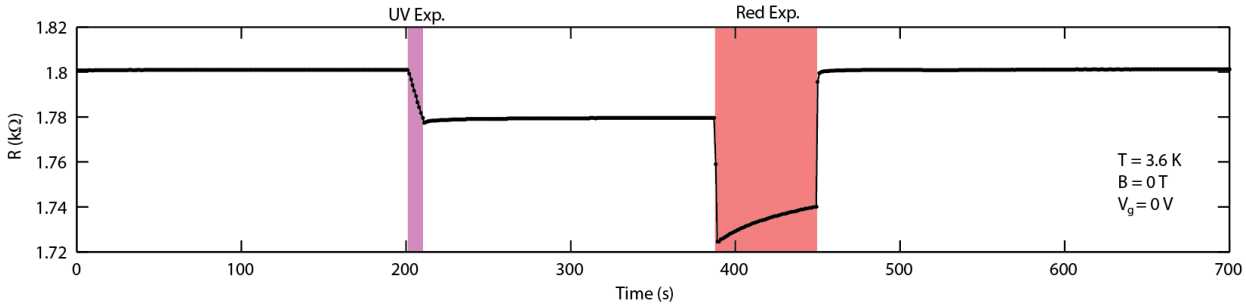

Figure S3. Optical gating of ≈ 50-nm sputtered ZnO film on $SrTiO_3$. Longitudinal resistance is plotted as a function of time during illumination by UV (purple highlighting) or red (pink highlighting) light, showing a persistent, bidirectional optical gating effect.

§ S4. Mechanism of the Optical Gating Effect

Optically-defined refractive structures have been studied for some time in $BaTiO_3$ and other perovskites and are attributed to selective optical redistribution of charged defects(*45*). In this photorefractive effect, the persistent electric field set up by defect population asymmetries modifies the refractive index of the material through (to first order) the Pockels effect(*29*). Though less commonly studied than other perovskites, photorefraction has been reported in both pure and Ca-doped $SrTiO_3$(*28*). We propose a gating mechanism which relies on analogous defect population dynamics, but in which the optical gradient is provided not only by intentional patterning, but also by the finite penetration depth into the crystal of light with energy above the band gap of $SrTiO_3$.

Consider a population of defects within the band gap of $SrTiO_3$ in a distribution of different charge states. Some may be donors and some may be acceptors. In the dark, the charges are bound to their defects. Upon illumination by light of sufficient energy E_d, charges are continuously excited into the bands and then recombine with the same or other nearby defects. If the crystal is exposed to light with energy above both E_d and above the bulk band gap E_g, (Figure S4A) it will penetrate only a finite distance into the crystal before being absorbed. Charges excited from defects in this optical gradient will undergo a similar cycle of photoexcitation and recombination, but if they happen to recombine farther into the crystal where the light intensity is lower, they will be less likely to be re-excited. This results in the eventual depopulation of charges from defect states near the surface of the crystal until all defects are affected or the electric field induced by this asymmetry balances the diffusive pressure of the optical gradient. When the light is switched off, all photoexcitation ceases and the charge distribution remains frozen in place. If illuminated again, but this time by light of energy between E_g and E_d, (Figure S4B) the light will penetrate through the entire sample, photoexciting defects throughout the crystal volume. In this case, recombination with nearby defects enables isotropic movement of charge, which allows any asymmetry to relax. The sign of the optical gating effect in our experiments is consistent with the accumulation of positive charge below the $(Bi,Sb)_2Te_3/SrTiO_3$ interface, which is the configuration shown in Figure S4A.

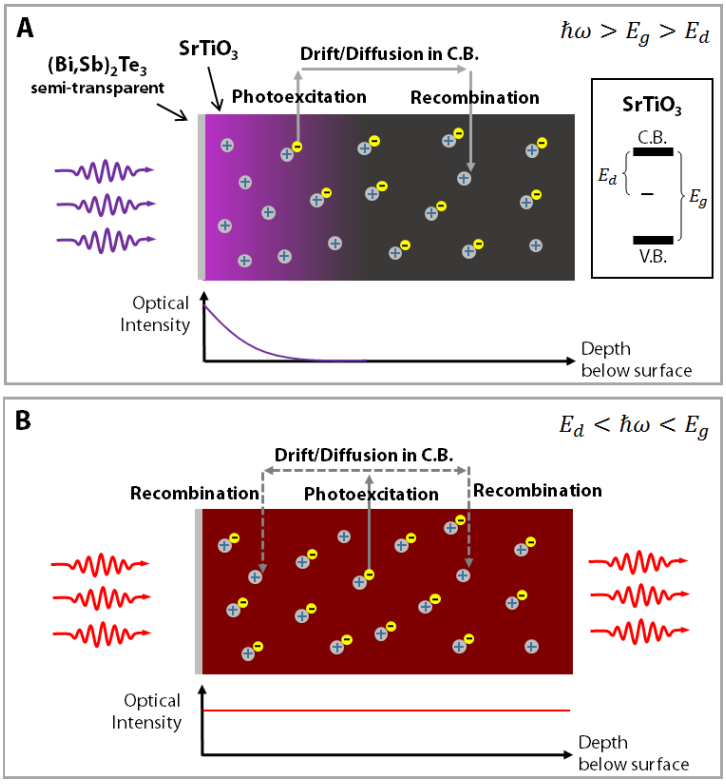

Figure S4. Mechanism of the optical gating effect. Schematic showing the near-surface distribution of charged defects with optical illumination above or below the band gap of $SrTiO_3$. **(A)** Light with energy above both the defect ionization energy E_d and bulk band gap E_g only reaches defects near the surface, which preferentially depopulates charge from this region. **(B)** Light with energy between E_g and E_d illuminates defects throughout the crystal volume, allowing population asymmetries to relax.

§ S5. Sample and Growth Characterization

Atomic Force Microscopy (AFM) was used to characterize the surface quality of each $SrTiO_3$ substrate after annealing, but before MBE growth. Figure S5A shows a typical substrate morphology with single atomic terraces on the order of at least 10 nm across and an RMS roughness of < 3 Å. The substrates were outgassed in the MBE chamber at a substrate temperature of 500 °C for about 1 hour before growth. $(Bi,Sb)_2Te_3$ was grown at a substrate temperature of ≈ 300 °C (pyrometer temperature of ≈ 215 °C) at a growth rate of about 0.3 QL per minute. Reflection high energy electron diffraction (RHEED) was used *in situ* in the MBE chamber to monitor the growth of the $(Bi,Sb)_2Te_3$ film (Figure S5B). The bright dot and concentric circles are from the direct beam. High angle annular dark field scanning transmission electron microscopy (HAADF-STEM) was used to image a cross-section of the interface with atomic resolution (Figure S5C). The $(Bi,Sb)_2Te_3$ film shows an ordered quintuple-layer structure, though an amorphous interfacial layer and some defects are visible. The carbon capping layer was applied to protect the sample during cross-sectional analysis, and is not present on the samples used in the optical experiments. Figure S5D shows X-ray diffraction (XRD) from a ≈ 10 QL thick film. The MBE growth and characterization of $(Bi,Sb)_2Te_3$ films, as well as their structural defects, are discussed in greater detail in a separate manuscript(*41*).

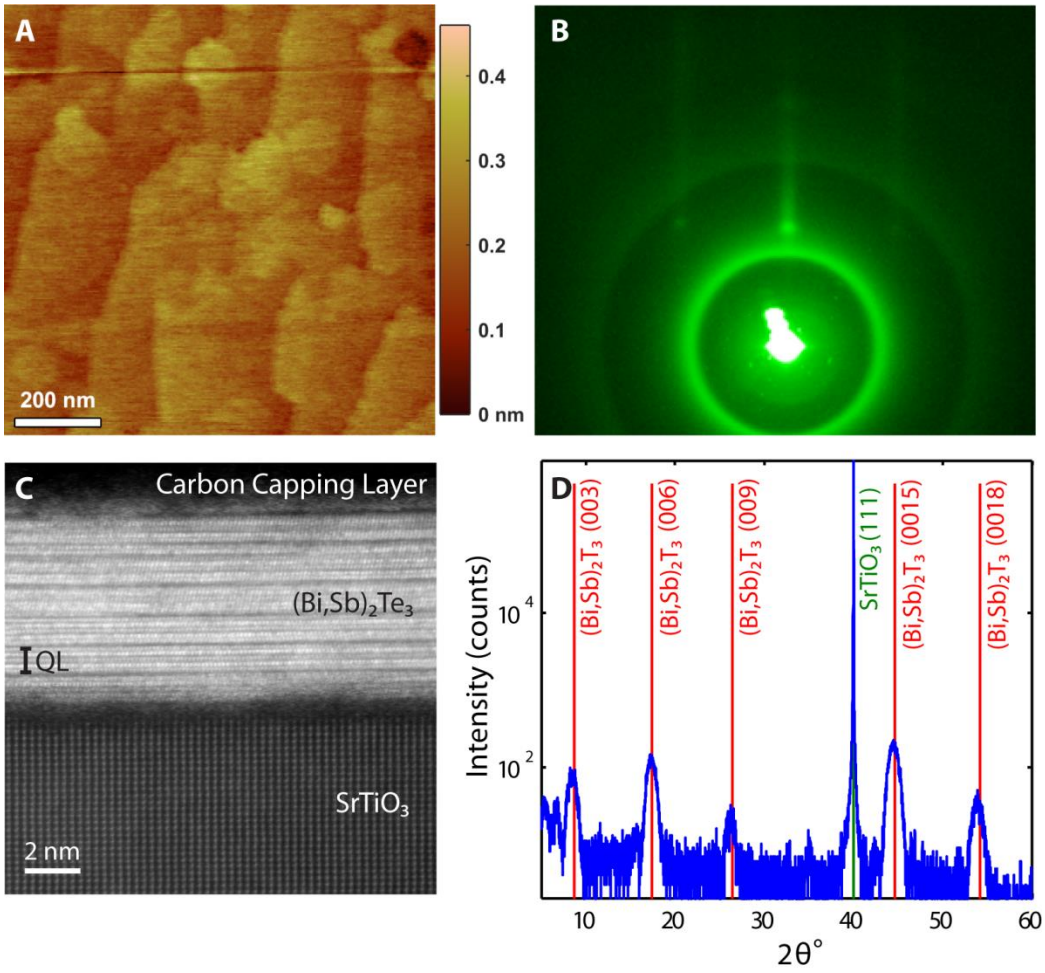

Figure S5. Sample growth and characterization. (A) AFM image of a representative $SrTiO_3$ substrate after annealing but before growth. **(B)** RHEED pattern observed after growth of a 6 QL $(Bi,Sb)_2Te_3$ film. **(C)** Cross-sectional HAADF-STEM image of 6 QL of $(Bi,Sb)_2Te_3$ grown on $SrTiO_3$. **(D)** XRD of a 10 QL sample after growth. The positions of the expected reflections for $(Bi,Sb)_2Te_3$ and SrTiO3 are labeled in red and green, respectively.